World Conference on Timber Engineering Oslo 2023

# INVESTIGATIONS ON SUITABLE LATERAL STIFFENING SYSTEMS FOR TALL TIMBER BUILDINGS

**Charles Binck[1], Andrea Frangi[2]**

**ABSTRACT:** As the height of timber buildings continues to increase, the importance of their lateral stiffness concept is growing. At present, the predominant structural system of timber buildings is a timber-concrete hybrid where the lateral stiffness of the building is provided by a reinforced concrete core. However, it is unknown which lateral stiffness concepts for tall timber building are feasible without the use of reinforced concrete. In this paper, five different lateral stiffening systems for tall timber buildings were investigated, with a focus on building heights between 50 and 230 meters. For this purpose, over 12 million building configurations were analysed with different lateral stiffening systems, and a design optimization was performed based on the dynamic response of the buildings subjected to wind loading. The study revealed that the development of semi-rigid connections for moment-resisting timber frames should target a stiffness ratio between 1% and 10% towards a fully rigid joint, to guaranty efficient connection solutions. For such connection stiffnesses, building heights of up to 190m may fulfil the serviceability criteria for cross-sections smaller than 40 x 120 cm.

**KEYWORDS:** Tall timber buildings, Lateral stiffening systems, Semi-rigid connections, Moment-resisting timber frames, Tube-in-tube systems, Serviceability criteria, Equivalent building stiffness, Height investigations.

## 1 INTRODUCTION

In the 20th century, buildings in steel and reinforced concrete saw rapid technological and engineering advancements. This enabled the construction of ground-breaking new tall buildings [1]. At present, a similar advancement for tall timber buildings is underway with ever-increasing building heights [2–4]. Two of the world's tallest timber buildings were built in Europe, namely the "HoHo" in Vienna at 84.0m and the "Mjøstårnet" in Brumunddal at 85.4m [5,6]. Since 2022, the tallest timber building is the "Ascent" in Milwaukee at 86.6m [4,7]. However, "Ascent" is constructed on a multi-storey reinforced concrete base [7,8].

As the buildings become taller, wind-induced serviceability vibrations and deflections become the governing design criteria. Here, the importance of the lateral stiffening system grows with increasing building heights. Currently, the predominant structural system is a timber-concrete hybrid where the lateral stiffness of the building is provided by a relatively stiff reinforced concrete core [4,8–10]. However, the use of reinforced concrete is a strong contributor to greenhouse gas emissions [11,12]. Consequently, there is a growing incentive to explore alternative solutions. Besides the promotion of renewable materials, other strong advantages of timber solutions are the lightness of the structures, the potential for a dry construction site and a shorter construction time.

While taller and taller timber buildings are being constructed, the development of feasible alternative lateral stiffness concepts comprising timber components has been stagnant. However, timber has the strength and stiffness to provide feasible solutions. Because of the unparalleled strength-to-weight ratio and similar stiffness-to-weight ratio of timber compared to other conventional building materials, competitive solutions can be provided for both the vertical and lateral load transfer. In Norway, both "Treet" in Bergen and "Mjøstårnet" in Brumunddal, demonstrate options for the lateral stiffening with bracing in the façade [6,13]. However, it is uncertain if other lateral stiffness concepts are feasible for tall timber buildings and which building heights could be achieved with these solutions.

For this purpose, the objective of this paper is to provide a comprehensive analysis of five different lateral stiffening systems, to explore their limits, and to present feasible solutions for building heights up to 190 meters. The systems are examined through more than 12 million simulations of unique building configurations subjected to service-level wind loading. The building configurations comprise different global and local geometries, material properties, mass, structural damping properties, joint stiffnesses, and serviceability criteria. In an analogy to the pioneering work of Fazlur Kahn on the premium for heights for steel and reinforced concrete buildings [14], this paper provides a guideline for current height limits of the lateral stiffening systems for tall timber buildings. The presented investigations of the different systems should be seen as a classification with feasible heights within the range of the chosen parameters and are not intended as boundaries outside this array.

[1] Charles Binck, Institute of Structural Engineering, ETH Zurich, 8093 Zurich, Switzerland, charles.binck@ibk.baug.ethz.ch
[2] Andrea Frangi, Institute of Structural Engineering, ETH Zurich, 8093 Zurich, Switzerland, frangi@ibk.baug.ethz.ch

https://doi.org/10.52202/069179-0386

## 2 THEORETICAL FRAMEWORK

### 2.1 STRUCTURAL TYPOLOGIES

Investigations were conducted on a braced inner core (Type I), an external frame tube in the façade (Type II), bracing systems in the façade (Type III and IV) and a tube-in-tube system with an external frame and an internal braced tube (Type V).

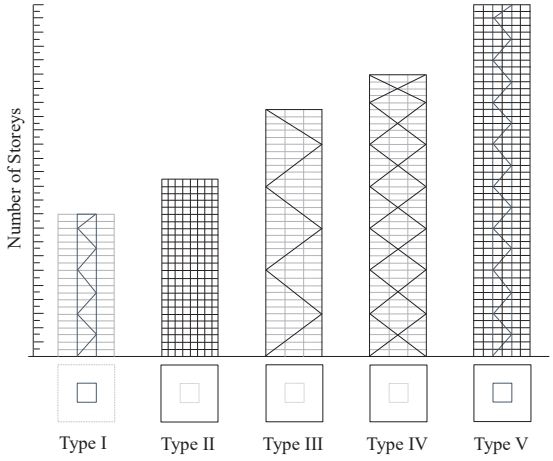


***Figure 1:*** *Overview of the investigated structural typologies based on the work of Fazlur Kahn* [14]

A description of the tube-in-tube concept is given in Binck et al. [15] where the system is illustrated in depth. By introducing moment-resisting connections, the timber parts, which are usually constructed as vertical load-bearing beam-column systems, may contribute substantially to the lateral stiffness. This would enable the beam-column structures to contribute with both vertical and lateral load-transfer.

### 2.2 PERFORMANCE CRITERIA

To assess the feasibility of the buildings, the serviceability criterion in ISO 10137 [16] based on occupant comfort is used. It is derived from measurements of buildings in vibration use. The serviceability criterion is for peak accelerations of offices or residential uses and is a function of the building's first natural frequency. In this paper, the stricter requirements for residential uses are used.

EN 1994-1-4 [17] provides in Annex B a framework to determine those accelerations and equivalent wind loads based on the gust factor approach for building heights up to 300 m height. In this paper, the basic wind velocity $v_{b,0}$ is 25 m/s. Accelerations are computed with subsequent computations based on a 1-year return period with a probability factor $c_{prob} = 0.73$.

In contrast to the accelerations, the peak deflections are calculated for a corresponding return period of 100 years by the static equivalent loads taking only the first mode into consideration. The higher return period is chosen here for a design criterion where damage on non-structural elements shall be avoided. In literature, there is no consensus or consistency for the criterion to avoid damage to non-structural elements [18,19]. However, current recommendations are in a range between $1/300$ to $1/1000$ of the building height for peak deflections and the inter-storey drifts [18,19]. Here, the performance criteria for peak deflections are set to a maximal global deflection of:

$$u_{peak} \leq \frac{H}{500} \tag{1}$$

for the building and a maximal inter-storey drift of:

$$\delta u_{peak} \leq \frac{h_s}{500}, \tag{2}$$

where $H$ and $h_s$ are the building height and the storey height respectively. The parameters used for the wind actions are summarised in Table 1.

***Table 1:*** *Overview of the parameters for the wind actions according to EN 1991-1-4 (2010).*

| Description | | $a_{peak}$ | $u_{peak}$ & $\delta u_{peak}$ |
|---|---|---|---|
| Actions computed according to | | EN 1991-1-4 (2010) Annex B | |
| Basic wind velocity | $v_{b0}$ | 25 m/s | |
| Return period | $R$ | 1 year | 100 years |
| Probability factor | $c_{prob}$ | 0.73 | 1.039 |
| Altitude factor | $c_{alt}$ | 1.0 | |
| Directional factor | $c_{dir}$ | 1.0 | |
| Seasonal factor | $c_{season}$ | 1.0 | |
| Turbulence factor | $k_1$ | 1.0 | |
| Air density | $\rho$ | 1.25 | |
| Reference height | $z_t$ | 200 m | |
| Reference length scale | $L_t$ | 300 m | |
| Minimum height | $z_{min}$ | 10 m | |
| Maximum height | $z_{max}$ | 200 m | |
| Roughness length | $z_0$ | 1.0 m | |
| Orography factor | $c_o$ | 1.0 | |
| Design criteria | | ISO 10137 | $H/500$ $h_s/500$ |

### 2.3 METHOD

#### 2.3.1 Finite Element Modelling

The structural analysis and simulations were conducted by adopting and expanding the finite element framework for assessing wind-induced vibrations for planar frames, first developed by Cao & Stamatopoulos [20–22]. In the framework, the trusses and beams use Euler-Bernoulli beam theory, and the columns use Timoshenko beam theory with a shear correction factor of 5/6. The beam-column connections are idealized as linear-elastic rotational springs with a stiffness $K_\theta$, the axial flexibility in the joints of the trusses is neglected, and the column-column joints are assumed to be rigid. More details can be found in Binck et al. [15] and Cao & Stamatopoulos [20–22].


https://doi.org/10.52202/069179-0386

### 2.3.2 Connection Stiffness

For a rigid beam-column joint, the equivalent rotational joint stiffness $K_{\theta,eq}$ can be derived by static condensation and expressed as:

$$K_{\theta,eq} = \frac{145EI_c}{6h} + \frac{239EI_b}{6l} + \frac{110EI_b^2 \cdot h}{6EI_c \cdot l^2} + 4\frac{EI_c^2 \cdot l}{EI_b \cdot h^2}, \quad (3)$$

where $h$ is the column height, $l$ is the bay length and $EI_c$ is the column stiffness and $EI_b$ is the beam stiffness, clarified in Figure 2. Hence, for a semi-rigid connection, the beam-column connection stiffness $K_\theta$ is defined as a fraction $\alpha_\theta$ of the equivalent beam-column joint stiffness $K_{\theta,eq}$:

$$K_\theta = \alpha_\theta \cdot K_{\theta,eq}, \quad (4)$$

Where $\alpha_\theta$ is the stiffness ratio and varies in the parameter study between 0.1 % and 100%. The connection stiffness $K_\theta$ can be illustrated as a reduced cross-section of the beam-column joint, as clarified in Binck et al. [15].

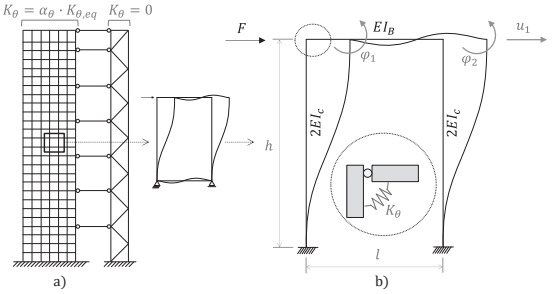


***Figure 2:*** *Structural system (a) and the statically equivalent model for determining the rotational stiffness (b).*

### 2.3.3 Equivalent Cantilever Stiffness

From a static perspective, a tall building can be illustrated as a vertical, encastered beam. By using this beam, the stiffness of the multi-degree-of-freedom system can be expressed in terms of a simple Timoshenko cantilever beam. This enables an easier expression and comparison of the different structural typologies in relation to the stiffness if an equivalent bending stiffness $EI_{eq}$ and shear stiffness $GA_{eq}$ can be determined. To find $EI_{eq}$, and $GA_{eq}$, the deformations can be decomposed as a superposition of the pure bending displacement $u_{EI}$, and pure shear displacement $u_{GA}$. Subsequently, the fraction of bending $\gamma_{EI}$ and shear $\gamma_{GA}$ contributions can be computed by linear regression.

With this approach, the analytical expression of the predicted displacement $u_{j,pred}$ can be written as:

$$u_{j,pred} = \gamma_{EI} \cdot u_j + \gamma_{GA} \cdot u_j. \quad (5)$$

By solving for $\gamma_{EI}$ and $\gamma_{GA}$, the fraction of bending displacement and shear displacement on the equivalent Timoshenko beam are determined and through the inverse procedure, the equivalent bending stiffness $EI_{eq}$ and shear stiffness $GA_{eq}$ can be derived.

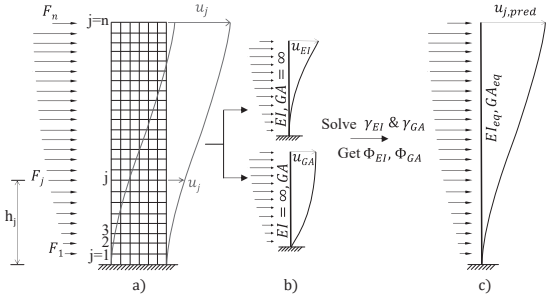


***Figure 3:*** *Model sketch of the mathematical procedure to determine the equivalent beam stiffnesses.*

An appropriate method to determine these stiffnesses for the equivalent cantilever beam, loaded by non-uniformly distributed loads, is the use of the curvature. The building displacements at storey height $h_j$ can be calculated as:

$$u_j = u_{j-1} + \delta u_j, \quad (6)$$

where $u_{j-1}$is the displacement from the storey below and $\delta u_j$ is the current storey drift, shown in Figure 4. This storey drift $\delta u_j$ is computed by curvature on the equivalent Timoshenko beam.

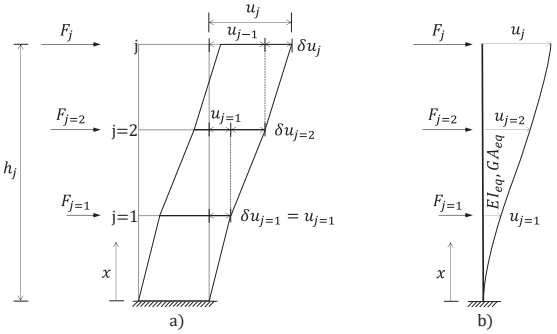


***Figure 4:*** *Calculation method of the deflections for the equivalent cantilever beam.*

For a homogeneous beam with a constant cross-section, the differential equation of a Timoshenko beam is given by:

$$EI_{eq}\frac{\delta^2\phi_y}{\delta x^2} - k_s GA_{eq}\left(\frac{\delta u_z}{\delta x} + \phi_y\right) = 0, \quad (7)$$

where $k_s$ is the Timoshenko shear coefficient, $\varphi_y$ is the curvature from pure bending, $\gamma_{xz} = -\varphi_y + \phi_y$ is the curvature from pure shear, and $\phi_y$ is the resulting angle of rotation from both, illustrated in Figure 5.

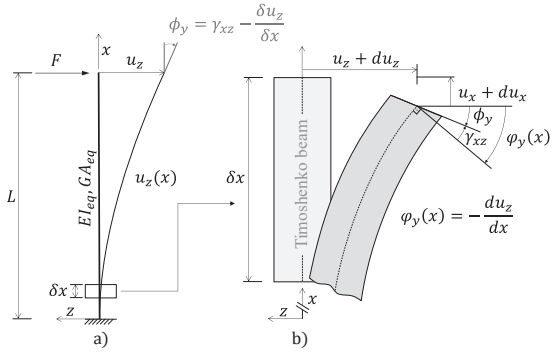


***Figure 5:*** *Applied Timoshenko beam theory.*

Internal forces in a beam are related to the strain, i.e., to the displacement $u$ and the rotation $\varphi_y$. For a linear elastic Timoshenko beam, the relations to the bending moment $M_y(x)$ and the shear force $Q_z$ are:

$$M_y(x) = -EI_{eq}\,\frac{\delta\phi_y}{\delta x}, \tag{8}$$

$$Q_z = k_s GA_{eq}\left(\frac{\delta u_z}{\delta x} + \phi_y\right). \tag{9}$$

For the cantilever beam, shown in Figure 5 a), where $x$ gives the positive direction from the clamped end to the free end, the bending moment $M_y(x)$ can be computed from the free-body diagram, as:

$$M_y(x) = F \cdot L - F \cdot x, \tag{10}$$

where $F$ is a point load at position $L$. Substituting Equation (9) into (7) gives:

$$EI_{eq}\frac{\delta\phi_y}{\delta x} = -F \cdot L + F \cdot x. \tag{11}$$

By integration, the bending curvature is written by:

$$\phi_y(x) = -\frac{1}{EI_{eq}}\left(F \cdot L \cdot x - \frac{1}{2}F \cdot x^2\right) + c_1, \tag{12}$$

where $c_1$ is a constant. Thus, substituting equation (12) into Equation (9), the total curvature of the Timoshenko beam can be expressed as:

$$\frac{\delta u_z}{\delta x} = \frac{Q_z}{k_s GA_{eq}} + \frac{1}{EI_y}\left(F \cdot L \cdot x - \frac{1}{2}F \cdot x^2\right) + c_1, \tag{13}$$

where the first part of the equation defines the curvature form pure shear and the second part defines the curvature from pure bending.

**Equivalent bending stiffness**

With Equation (12), the equivalent bending stiffness of a multi-storey building under nonuniform distributed loads can be written as:

$$EI_{eq} = \frac{1}{\frac{\delta u_{j,EI}}{\delta x}} \cdot \left[F_j \cdot \left(h_j \cdot x - \frac{1}{2}x^2\right) + c_{j,EI}\right], \tag{14}$$

where $c_{j,EI}$ is a constant resulting from the curvature at level j as a consequence of the actions below:

$$c_{j,EI} = F_{j-1} \cdot \left(h_{j-1} \cdot x - \frac{1}{2}x^2\right) + c_{j-1}. \tag{15}$$

Equations (14) and (15) show, that the bending curvature at storey $j$ refers to the curvatures and loads from the entire building and indicate the advantage of computer aided calculations. Finally, the inter-storey drift $\delta u_j$ is written by:

$$\delta u_j = \frac{\delta u_j}{\delta x} \cdot h_j - \frac{\delta u_j}{\delta x} \cdot h_{j-1}. \tag{16}$$

**Shear stiffness**

In analogy to the bending stiffness, the shear stiffness is derived by Equation (13) to:

$$GA_{eq} = \frac{Q_z \cdot x}{\delta u_{j,GA}}, \tag{17}$$

where $Q_z$ is the shear force and thus the sum of the non-uniformly distributed loads above the height $x$:

$$Q_z = \sum_{i=j}^{n} F_i. \tag{18}$$

**Equivalent cantilever stiffness**

With the bending stiffness and shear stiffness, the equivalent beam stiffness can be computed by:

$$K_{B,eq} = \left(\frac{1}{K_{EI,eq}} + \frac{1}{K_{GA,eq}}\right)^{-1}, \tag{19}$$

where:

$$K_{EI,eq} = \frac{3EI_{eq}}{H^3}\ , \quad K_{GA,eq} = \frac{GA_{eq}}{H}. \tag{20}$$

## 3 PARAMETER STUDY

The parameters are chosen to cover the most realistic variations of the building geometry. Because of the high number of possible configurations, over 12 million simulations are analysed. The varying parameters are the number of stories $n_s$, number of bays $n_b$, bay length $l_b$, column cross-sections $b_c \times h_c$, beam cross sections $b_b \times h_c$, bracing cross-sections $b_{br} \times h_{br}$, rotational stiffness ratio of the beam-column joints $\alpha_\theta$, glued laminated timber strength grades between GL28h and GL75, characteristic storey loads $p_s$, the internal core ratio $\beta$, which is the ratio between the external tube $B$ and the internal tube $L_{br}$, logarithmic decrement of the structural damping $\delta_s$ and the return period $R$ for the basic wind speed. The mass of the building is assumed to be uniformly distributed along the height of the buildings. Figure 6 shows the parameters graphically.


https://doi.org/10.52202/069179-0386

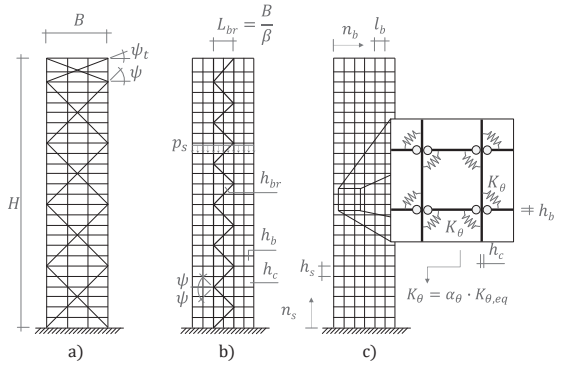


***Figure 6:*** *Illustration of the parameters.*

The constant parameters are the storey height $h_s$ which is fixed at 3.5 m. The bracing angle $\psi$ is variable and determined by the building width and internal core width. However, $\psi$ is approximately 45° and is optimised to find the closest storey, to connect centred to the beam-column-joint. $\psi_t$ is the resulting bracing angle of the top bracing. Table 2 summarises the parameters for the structural investigations. The investigations on the Type II and on the Type V are constant member widths $b_{c,b,br}$, of 0.4m. Here, only the member heights $h_{c,b,br}$ are paramterised and vary between 0.4m and 1.2m. For the braced systems in Type I, III, and IV, the brace cross-sections are square.

***Table 2:*** *Overview of the parameters for the structural investigations*

| Structure Typology | | Frame (Type II) | | | Bracing (Type I, III, IV) | | | Tube-in-Tube (Type V) | | | |
|---|---|---|---|---|---|---|---|---|---|---|---|
| | | Min | Max | Step | Min | Max | Step | Min | Max | Step | Unit |
| Number of bays | $n_b$ | 6.00 | 12.00 | 2.0 | 6.00 | 12.00 | 2.0 | 6.00 | 12.00 | 2.0 | - |
| Bay width | $l_b$ | 2.40 | 4.20 | 0.6 | 2.40 | 4.20 | 0.6 | 2.40 | 4.20 | 0.6 | m |
| Number of storeys | $n_s$ | 15 | 65 | 5.0 | 15 | 65 | 5.0 | 15 | 65 | 5.0 | m |
| Column width | $b_c$ | 0.40 | 0.40 | - | 0.40 | 1.20 | 0.20 | 0.40 | 0.40 | - | m |
| Column height | $h_c$ | 0.40 | 1.20 | 0.20 | 0.40 | 1.20 | 0.20 | 0.40 | 1.20 | 0.20 | m |
| Beam width | $b_b$ | 0.40 | 0.40 | - | - | - | - | 0.40 | 0.40 | - | m |
| Beam height | $h_b$ | 0.40 | 1.20 | 0.20 | - | - | - | 0.40 | 1.20 | 0.20 | m |
| Bracing width | $b_{br}$ | - | - | - | 0.40 | 0.40 | - | 0.40 | 0.40 | - | m |
| Bracing height | $h_{br}$ | - | - | - | 0.40 | 1.20 | 0.20 | 0.40 | 1.20 | 0.20 | m |
| Surface load/storey | $p_s$ | 5 | 10 | 2.5 | 5 | 10 | 2.5 | 5 | 10 | 2.5 | kN/m$^2$ |
| Rotational stiffness ratio | $\alpha_\theta$ | 0.1 | 100 | ([a]) | 1 | 100 | ([a]) | 1 | 100 | ([a]) | % |
| Material | | GL28h[(b)] | GL75[(d)] | GL48h[(c)] | GL28h | GL75 | GL48h | GL28h | GL75 | GL48h | - |
| Internal core ratio | $\beta$ | - | - | - | 1 | 3 | 0.5 | 1 | 3 | 0.5 | - |
| Structural damping | $\delta_s$ | 0.1 | 0.5 | 0.1 | 0.1 | 0.5 | 0.1 | 0.1 | 0.5 | 0.1 | - |

([a]) the rotational stiffness of the moment resisting connection is changed unregularly by the following steps: $\alpha_\theta$ = 0.1, 0.25, 0.5, 1.0, 2.5, 5.0, 10, 25, 50 100%.
([b]) GL28h according EN 14080 [23] with $E$=12'600N/mm$^2$ and $G$=650N/mm$^2$
([c]) GL48h for hardwood GLT according Neue Holzbau AG [24] with $E$=15'000N/mm$^2$ and $G$=1000N/mm$^2$
([d]) GL75 for Pollmeier Baubuche according [25] with $E$=16'800N/mm$^2$ and $G$=850N/mm$^2$

## 4 RESULTS AND DISCUSSION

### 4.1 EQUIVALENT CANTILEVER STIFFNESS

The equivalent stiffness approach in Section 2.3.3, enables the comparison of the different structural systems in terms of the global building stiffness. Independent from the lateral stiffening, the equivalent cantilever beam can quantify the building stiffness. For all the simulations, the coefficient of determination $R^2$ from the deflections of the finite element results and the predicted deflections of the equivalent cantilever beam is between 0.975 and 1.0. The approach is promising and enables the structural typologies to be assessed in terms of their serviceability.

Based on the results, the varying systems can be analysed towards their bending and shear stiffnesses. Figure 7 shows the scatter of the equivalent bending stiffness $EI_{eq}$ in relation to the equivalent shear stiffness $GA_{eq}$, where both, horizontal and vertical axis are shown on the base-10 logarithmic scale. In the figure, a set of the results is shown which fulfil the serviceability criteria from Section 2.2 and reveals a slenderness of $H/B > 3.0$. In addition, the plotted results are computed for member grades in GL28h. For the frames and tube-in-tube systems, Figure 7 only presents results for rotational connection stiffness with $\alpha_\theta \leq 1.0$ % and internal core dimensions with $\beta_{br} = 3.0$, i.e. $L_{br} = 1/3 \cdot B$ for Type I and Type V.

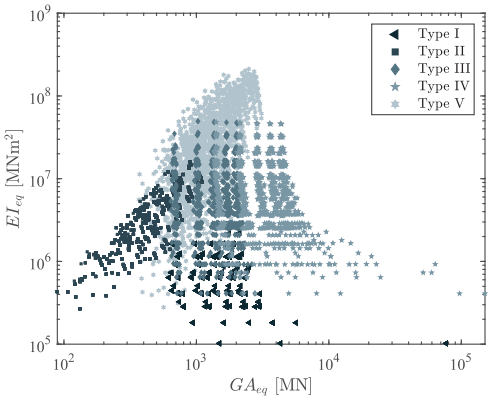


***Figure 7:*** *Behaviour between the equivalent bending stiffness $EI_{eq}$ and shear stiffness $GA_{eq}$.*

The relation between $EI_{eq}$ and $GA_{eq}$ reveals the strengths and weaknesses of the different systems. Knowing that the frames are more shear compliant than bracings, Figure 7 proves that the tube-in-tube systems as combined configurations achieve bending stiffnesses in the order of braced systems in the façade.

Figure 8 highlights the study resulted building stiffnesses from above in a swarm chart. The figure can be used as a qualitative assessment, to assess the different systems on their global stiffnesses according to the frequency of the results. For all types, the results are visualised in Figure 8 with their distribution of the achieved stiffnesses.

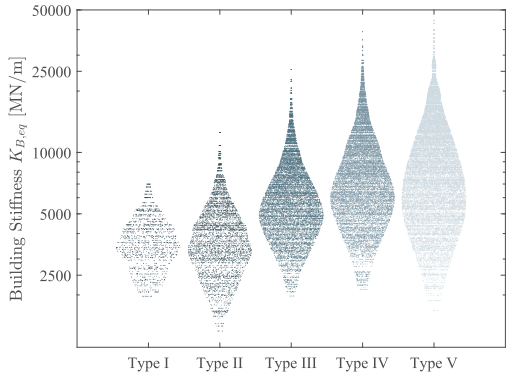


***Figure 8:*** *Equivalent building stiffnesses of the different systems for a set of simulations.*

## 4.2 ROTATIONAL CONNECTION STIFFNESS

Figure 9 shows the relation of the equivalent rotational joint stiffness $K_{\theta,eq}$ and the bay length $l_b$, the storey height $h_s$ and varying beam dimensions.

It is apparent from Figure 9 that the storey height $h_s$ becomes less significant with increasing bay lengths $l_b$. Its impact is smaller in comparison to the bay lengths $l_b$, the cross-sections of the members $b_b \times h_b$, $b_c \times h_c$, and the young's modulus $E$. However, the storey height $h_s$ is not negligible, particularly for small bay lengths. For beams which are weaker than the columns, the impact of the bay length $l_b$ diminish and the influence of the storey height $h_s$ is approximately constant for increasing bay lengths. This can be seen in Figure 9.

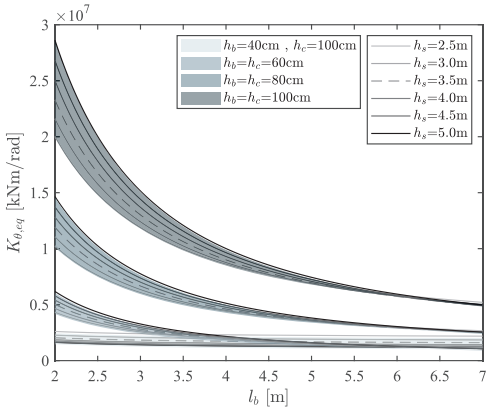


***Figure 9:*** *Relation of the equivalent rotational joint stiffness $K_{\theta,eq}$, bay length $l_b$, storey height $h_s$ and member cross-sections.*

Since the beam-column connection stiffness $K_\theta$ is only a fraction $\alpha_\theta$ of the equivalent rotational joint stiffness $K_{\theta,eq}$, as expressed in Equation (4), it is appropriate to identify the impact of the joint stiffness in relation to the building stiffness.

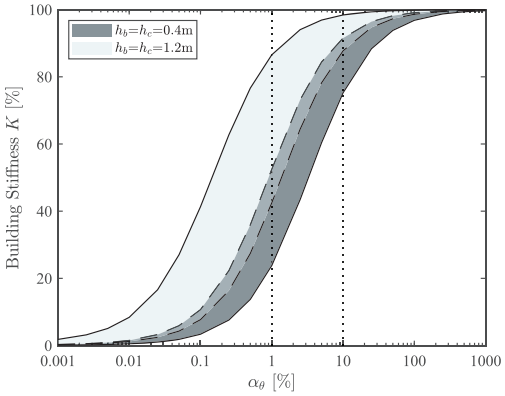


***Figure 10:*** *Impact of the connection stiffness on the global building stiffness. $\alpha_\theta$ is plotted on the logarithmic scale to clarify the increase of the building stiffness in the smaller range.*

Figure 10 presents the behaviour of the building stiffness $K$ in relation to the connection stiffness ratio $\alpha_\theta$ for a wide range of parameters. The building stiffness $K$ on the vertical axis is here illustrated as the fraction of the equivalent beam stiffness $K_{B,eq}$ towards a fully rigid moment resistant frame to normalise the results. Hence, the building stiffness is expressed in percent:

$$K = \frac{K_{B,eq}(\alpha_{\theta,i})}{K_{B,eq}(\alpha_\theta = 100\%)} \tag{21}$$

The hatched areas in the figure contain all possible combination for the varying parameter configurations,


https://doi.org/10.52202/069179-0386

where configurations with the smallest member cross-sections $h_b$=$h_c$=40cm and larges cross-sections $h_b$=$h_c$=120cm are subdivided.

Figure 10 reveals, that the beam-column connection stiffness $K_\theta$ has a large impact on the building stiffness when the stiffness ratio $\alpha_\theta$ is within the range of 0.01% to about 10%. For stiffness ratios $\alpha_\theta$ of more than 10%, the impact is smaller because of the exceedingly high values of $K_\theta$ and the large number of beam-column joints. A stiffness ratio $\alpha_\theta$ of 5% in the beam-column joints results in a global lateral stiffness $K$ between 60% and 98% when compared with an equivalent building with rigid beam-column joints. Whereas slender beams need higher connection stiffnesses than stiffer or larger beams, to achieve maximal building stiffnesses.

So, for instances, achieves a building with a framed tube (Type II) in GL28h with $n_b$=6 bays, bay lengths $l_b$=3.6m, $n_s$=25 storeys, storey height $h_s$=3.5m, beam and columns cross-sections of $b_b \times h_b$=40×100cm and $b_c \times h_c$=40×60cm a global lateral building stiffness of $K$=79% for a connection stiffness ratio of $\alpha_\theta$=1.0%. Whereas the same building with a relatively equal stiffness ratio $\alpha_\theta$=1.0%, but with reversed member dimensions, i.e., beam cross-sections $b_b \times h_b$=40×60cm and columns $b_c \times h_c$=40×100cm, only achieves a global building stiffness of $K$=32%. Figure 11 shows, that only a small $\alpha_\theta$ is needed to provide stiff connections as peak accelerations and deflections are only slightly affected after a certain achieved rotational stiffness. For the illustrated 25 multi-storey frame, the gain with connection stiffness ratios $\alpha_\theta$ above 1% is marginal.

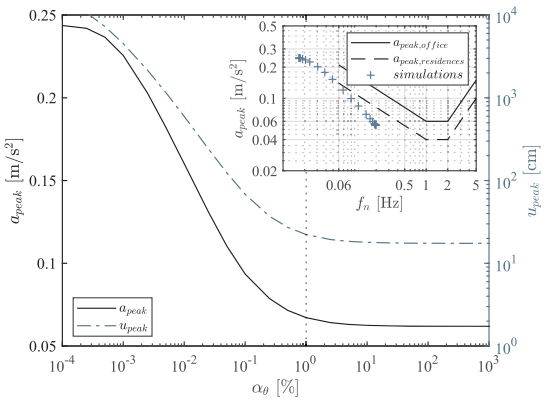


***Figure 11:*** *Behaviour of the peak accelerations and peak displacements related to the rotational connection stiffness for an illustrative external frame (Type II) in GL28h with 25 storeys, 6×3.6m bays, storey height 3.5 m, $\delta_s$=0.1, beam cross-sections 40×100cm and column cross-sections 40×60cm.*

Apart from slender beams, an increase of the stiffness ratio $\alpha_\theta$ above 10% is in general not worthwhile. Consequently, the development of semi-rigid beam-column joints should target a stiffness ratio $\alpha_\theta$ between 1% and 10% to guarantee efficient solutions. Such stiffness ratios result in stiffnesses, which are high and currently challenging in timber to achieve. However, they are not impossible. Considering the mentioned building above for instances, where beam and column cross-sections are $b_b \times h_b$=40×100cm and $b_c \times h_c$=40×60cm, bay length $l_b$ is 3.6m, storey height $h_s$ is 3.5m, and the elastic modulus $E$ is 12'600N/mm², then, a stiffness ratio $\alpha_\theta$=1% results in a rotational stiffness $K_\theta$ of 242'150kNm/rad. Through experimental and analytical considerations Stamatopoulos et al. [26] showed that their current system based on threaded rods results in rotational stiffness ratios $\alpha_\theta$ in the order of 2.3%, when the connections would be applied in the mentioned building. Their investigations proved a connection stiffness $K_\theta$ in the order of 7618kNm/rad for two threaded rods in plane with members in GL30c and cross-sections of $b_b/h_b$=14/45cm and $b_c/h_c$=14/45cm respectively. From an engineering point of view, these results indicate that multi-storey frame structures could enable a new era of tall timber buildings, when combined with an internal core, as will be shown in the following.

### 4.3 SERVICEABILITY STUDY

The wide-ranging parameter study enables the sensitivity analysis on the significance of the different parameters. The impact and weight of the varying parameters are described in depth in Binck et. al. [15]. Towards the serviceability limit state, the most important parameters of the different systems are the rotational connection stiffness $K_\theta$ while stiffness ratios $\alpha_\theta$ are under 10%, the member dimensions $b_{b,c,br}$ and $h_{b,c,br}$, the timber grades and the number of bays $n_b$ which have a higher importance than the bay length $l_b$ and storey height $h_s$. In contrast to the peak displacements, the mass, its distribution, and the damping properties have a pronounced importance on the peak accelerations.

To assess the height limitations of the different stiffening systems, the structures are subjected to the performance criteria, presented in section 2.2. Depending on the varying parameters, the height limit is defined for the tallest structures, which still fulfil all three, the peak acceleration criterion $a_{peak}$, the peak displacement criterion $u_{peak}$, and the maximum inter-storey drift $\delta u_{peak}$ criteria.

For the structural types II, IV and V, Figure 12 shows the structural height limitations with the dashed grey line. The limits are expressed in terms of the maximum storey number and the common parameters. If the peak displacement criteria are the decisive criteria, the height limit is plotted trough the grey circled markers. The grey markers indicate the ultimate storey number for the satisfaction of the displacement criteria. If the acceleration criterion is the decisive criterion, the decision line pass through the black, squared markers. For the latter, the requirements for residential uses according ISO 10137 [16] are assessed.

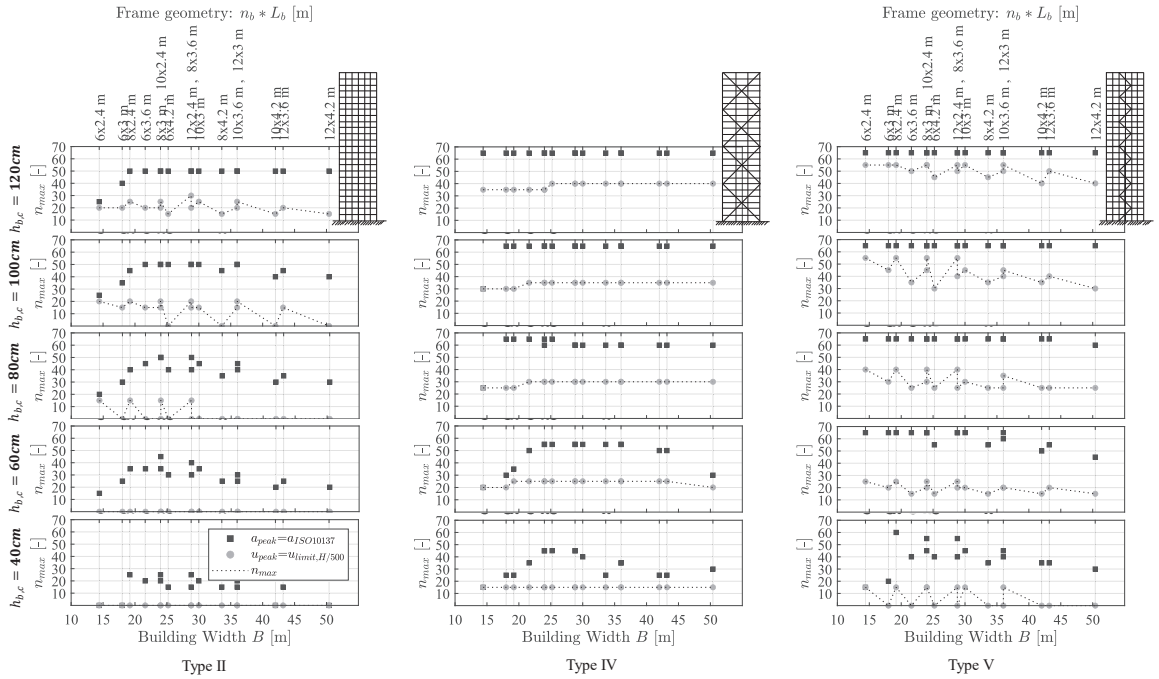


***Figure 12:*** *Height investigations of Types II, IV and V which fulfil the serviceability criteria, expressed in terms of the storey number $n_{max}$. The common parameters for the shown results are the glued laminated timber strength grades in GL28h for all members, constant characteristic storey loads of $p_s$=7.5kN/m², storey height $h_s$=3.5m, structural logarithmic damping decrements of $\delta s$=0.1, rotational connections stiffnesses of $\alpha_\theta$=1.0% for the semi-rigid connections and beam and bracing cross-sections of 1) $b_{b,br} \times h_{b,br}$=40×40cm, 2) $b_{b,br} \times h_{b,br}$=40×60cm, 3) ) $b_{b,br} \times h_{b,br}$=40×80cm, 4) ) $b_{b,br} \times h_{b,br}$=40×100cm, 5) ) $b_{b,br} \times h_{b,br}$=40×120cm in the different figures. Type II and V have same column cross-sections. For type IV, the column cross-sections are squared, thus 1) $b_{b,br} \times h_{b,br}$= 40×40cm, 2) $b_{b,br} \times h_{b,br}$=60×60cm, 3) $b_{b,br} \times h_{b,br}$=80×80cm, 4) $b_{b,br} \times h_{b,br}$=100×100cm, 5) $b_{b,br} \times h_{b,br}$=120×120cm.*

Figure 12 reveals the relevance of the displacement criteria for various parameters. In general, three main reasons indicate the relevance of the displacement criteria: first, the small young's modulus $E$ of GL28h leads to relatively weak structures, compared to other materials. This is also a reason for why the height limits for increasing building widths are constant. Regarding the increasing wind contact surface which larger buildings provide, the strains in the extensive large members mount up to large deformations. Only a simultaneous increase of the member cross-sections enables deflection reductions in that case. The second reason is the relatively high storey load for the comparatively weak structures, which is here set to $p_s$=7.5kN/m² as a characteristic load and corresponds to a building density of about 214 kg/m³ including all dead loads and quasi permanent live loads. For lightweight buildings with storey loads of 5.0 kN/m² for instances, the acceleration criterion becomes frequently the governing criterion. Finally, the third reason is the calculation for the higher return period of 100 years for the displacements.

## 4.4 HEIGHT INVESTIGATIONS

Based on Figure 12, the determination of the height limits for the structural timber systems is carried out for all parameter configurations. Analogously, Figure 13 summarises the achievable heights for all investigations with varying parameters listed in Table 1 and Table 2. Here the results are valid for the fixed parameters with a constant storey height $h_s$=3.5m, a logarithmic damping decrement of the structure $\delta_s$=0.1 and constant characteristic storey loads of $p_s$=7.5kN/m². In Figure 13, the current height limits for GL28h are presented:

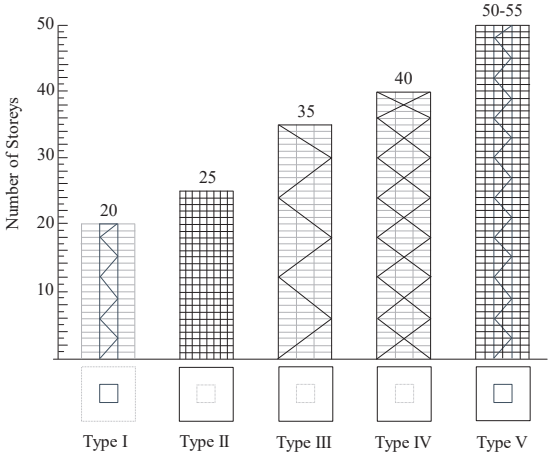


***Figure 13:*** *Height investigations for structural timber systems subjected to wind loading.*


https://doi.org/10.52202/069179-0386

From a serviceability point of view, the results indicate that the braced systems in the façade (Type III and IV) and the tube-in-tube systems (Type V) presents feasible solutions for building heights $H$>100m. Considering the requirements of $u_{peak} \leq H/500$, $\delta u_{peak} \leq h_s/500$ and the acceleration criterion in ISO 10137 [16] as comfort criteria, the structures perform well up to 140m for Type IV and 175m-190m for Type V with storey heights $h_s$=3.5m. However, this should be seen more as a guideline than as a stringent boundary. Regarding the serviceability, investigations on higher structures are feasible when larger cross-section will be guaranteed to provide the required stiffnesses.

The advantage of Type V as a tube-in-tube system would be the use of the existing structure from the vertical load transfer while applying simultaneously to the horizontal load transfer, without adding further members in the façade layer. However, high demands are made on the moment-resisting connections as they have to act as key elements to provide the required stiffnesses. At present, these connections are still challenging because of the anisotropic material properties, and their development has just begun. Moment-resisting connections are no common solutions in timber structures but could enable a new field for tall timber buildings.

## 5 CONCLUSIONS

At present, the predominant structural system for tall timber buildings is a hybrid solution, where a reinforced concrete core provides the lateral stiffness. To assess alternative solutions in timber, five different systems were analysed in this paper to assess the performance of lateral stiffening systems in timber. The main goal was to explore the feasible heights of timber solutions for the presented systems.

Based on a parameter study, the classification of efficient height limits was induced on the lateral stiffness capabilities for wind induced vibrations. The structural typologies have been compared with respect to their stiffness and analysed for peak accelerations and displacement limitations. The height indications have not been analysed and classified according to the ultimate limit state.

With an efficient and well-designed lateral stiffening system, holistic timber buildings can satisfy the acceleration requirements for residential uses according to ISO 10137 and the peak displacement criteria of $u_{peak} \leq H/500$ and $\delta u_{peak} \leq h_s/500$ for a 100 year return period. There is a great potential for timber solutions that will allow buildings to reach heights up to 190m. This potential is dependent by a wide range of parameters and is presented for a certain parameter range in this paper. The key takeaway from the analysed structures should be, that the wind induced deformations are in most cases the decisive requirement while assessing the displacement criteria to $u_{peak} \leq H/500$ at the head deflections and $\delta u_{peak} \leq h_s/500$ for the inter-storey drift.

The comparison can be seen as a fundamental research for height investigations for a new era of timber buildings in terms of different structural systems. This will enable a more global perspective of quantifying the lateral stiffness for tall timber buildings to enforce its structural design. However, a more in-depth study is needed to include the structural analysis on the ultimate limit state in order to provide a holistic assessment on the ultimate height limitations and to identify the “premium for heights”.

## ACKNOWLEDGEMENT

This article is written within the framework of the project “Lateral Stiffening Systems For Tall Timber Buildings”. The authors gratefully acknowledge the funding from Innosuisse – Swiss Innovation Agency. Special thanks also go to the project partners Schnetzer Puskas Ingenieure AG and Boltshauser Architekten AG.

## REFERENCES

[1] Tamboli AR. Tall and supertall buildings : planning and design. New York: Mcgraw-Hill Education; 2014.

[2] Svatoš-Ražnjević H, Orozco L, Menges A. Advanced Timber Construction Industry: A Review of 350 Multi-Storey Timber Projects from 2000–2021. Buildings 2022;12:404. https://doi.org/10.3390/buildings12040404.

[3] Kuzmanovska I, Gasparri E, Tapias Monne D, Aitchison M. Tall timber buildings: Emerging trends and typologies. World Conference on Timber Engineering (WCTE 2018), Seoul, Korea, Republic Of.: 2018.

[4] Safarik D, Elbrecht J, Miranda W. State of Tall Timber 2022. Council on Tall Buildings and Urban Habitat, CTBUH Research Journal 2022;1:22–9.

[5] Woschitz R, Zotter J. Holzhochhaus HoHo Wien - Das Tragwerkskonzept. Österreichische Ingenieur- Und Architekten-Zeitschrift 2017;162.

[6] Abrahamsen R. Mjøstårnet-18 storey timber building completed. 24 Internationales Holzbau-Forum IHF 2018.

[7] Thornton Tomasetti. Project Ascent 2023. https://www.thorntontomasetti.com/project/ascent (accessed March 14, 2023).

[8] Fernandez A, Komp J, Peronto J. Ascent - Challenges and Advances of Tall Mass Timber Construction. International Journal of High-Rise Buildings 2020;9:235–44. https://doi.org/https://doi.org/10.21022/IJHRB.2020.9.3.235.

[9] Jung P. Suurstoffi BF1 Rotkreuz: 60Meter – 15 Geschosse – 15 Wochen. 24. Internationales Holzbau-Forum IHF 2018, Internationales Holzbau-Forum IHF; 2018, p. 1–12.

[10] Vola M, Verhaegn R, de Jong J. Haut - A 21-storey Tall Timber Residential Building. International Journal of High-Rise Buildings 2020;9:213–20. https://doi.org/https://doi.org/10.21022/IJHRB.2020.9.3.213.

[11] International Energy Agency (IEA). Technology Roadmap - Low-Carbon Transition in the Cement Industry. Paris: 2018.
[12] Bellmann E, Zimmermann P. Klimaschutz in der Beton- und Zementindustrie - Hintergrund und Handlungsoptionen. Berlin: 2019.
[13] Malo KA, Abrahamsen RB, Bjertnæs MA. Some structural design issues of the 14-storey timber framed building "Treet" in Norway. European Journal of Wood and Wood Products 2016;74:407–24. https://doi.org/10.1007/s00107-016-1022-5.
[14] Ali MM, Moon KS. Structural Developments in Tall Buildings: Current Trends and Future Prospects. Archit Sci Rev 2007;50:205–23. https://doi.org/10.3763/asre.2007.5027.
[15] Binck C, Cao AS, Frangi A. Lateral stiffening systems for tall timber buildings – tube-in-tube systems. Wood Mater Sci Eng 2022:1–8. https://doi.org/10.1080/17480272.2022.2086066.
[16] ISO. ISO 10137-2007. Bases for design of structures - Serviceability of buildings and walkways against vibrations. 2007.
[17] CEN. EN 1991-1-4 Eurocode 1: Actions on structures - Part 1-4: General actions -Wind actions. In: European Committee for Standardization, editor., 2010.
[18] Griffis LG. Serviceability Limit States Under Wind Load. Engineering Journal, American Institute of Steel Construction 1993;30:1–16.
[19] Smith R. Deflection Limits in Tall Buildings—Are They Useful? Structures Congress 2011, Reston, VA: American Society of Civil Engineers; 2011, p. 515–27. https://doi.org/10.1061/41171(401)45.
[20] Cao AS. Dynamic response of semi-rigid timber frames subjected to wind loads. Masterthesis. Norwegian University of Science and Technology, 2020.
[21] Cao AS, Stamatopoulos H. A theoretical study of the dynamic response of planar timber frames with semi-rigid moment-resisting connections subjected to wind loads. Eng Struct 2021;240:112367. https://doi.org/https://doi.org/10.1016/j.engstruct.2021.112367.
[22] Cao AS, Stamatopoulos H. Theoretical studies of tall timber buildings subjected to service-level wind loads. World Conference on Timber Engineering (WCTE 2021) 2021:1964–9. https://doi.org/10.3929/ethz-b-000507921.
[23] CEN. EN 14080 Timber structures - Glued laminated timber and glued solid timber - Requirements. 2013.
[24] Neue Holzbau AG. Eigenschaften Brettschichtholz in Laubholz. Lungern: 2020.
[25] Österreichisches Institut für Bautechnik (OIB). ETA-14/0345. Wien: 2021.
[26] Stamatopoulos H, Malo KA, Vilguts A. Moment-resisting beam-to-column timber connections with inclined threaded rods: Structural concept and analysis by use of the component method. Constr Build Mater 2022;322:126481. https://doi.org/10.1016/j.conbuildmat.2022.126481.


https://doi.org/10.52202/069179-0386